journal

J. Am. Ceram. Soc., 97 [12] 3853–3856 (2014)
DOI: 10.1111/jace.13230

Quantitative Characterization of Mechanical Stress Field and Fracture Strength in Isotropic Brittle Materials During Crack Tip Propagation

Roberto Dugnani,[‡,†] and Ricardo J. Zednik[§]

[‡]University of Michigan - Shanghai Jiao Tong University Joint Institute, 800 Dong Chuan Road, Shanghai 200240, China

[§]École de Technologie Supérieure, Université du Québec, Montréal, Canada

A generalized method for characterizing mechanical stresses in brittle materials during crack tip propagation is presented. This approach was derived from classical fracture mechanics and is therefore mechanism independent and applies to any isotropic brittle material, including glasses, fine grained ceramics or metals, and high stiffness polymers. A practical implementation demonstrates the merits of this technique: the fracture strength can be determined by characterizing the angle between the free surface of a flexural overload fracture and stress intensity factor loci. The accuracy of this method was phenomenologically validated using flexural strength tests on glass as a model material system. In addition, such fractographic measurements can also be used to characterize an inhomogeneous internal stress field, and thereby, for example, help discriminate whether the sample failed due to pure bending loads alone, or whether membrane stresses were also present.

I. Introduction

The ability to characterize mechanical stresses in isotropic brittle materials during crack tip propagation is of paramount importance in fracture mechanics. An experimental *in-situ* measurement during crack growth is practically challenging, because either the crack tip cannot be readily imaged during propagation or the fracture event occurred in the past. Therefore, a generalized method for retroactively determining the mechanical stress state during propagation of the crack tip by studying the resulting fracture surface is particularly valuable.

We derive such a generalized method by employing classical fracture mechanics principles applicable to any isotropic brittle material, including glasses, fine grained ceramics or metals, and high stiffness amorphous polymers. In this manuscript, we leverage a practical example to better illustrate the derivation and implementation of our method: determining the stresses in an isotropic brittle material by characterizing the angle between the free surface and stress intensity factor (SIF) loci in bending overload.

During an overload event, the fracture surface roughness typically increases as the crack tip accelerates through the material. We can define a "mirror" region corresponding to the fracture surface that is optically reflective, as it has a roughness below the wavelength of visible light. When the crack tip propagates and its surface roughness reaches the wavelength of visible light, light is scattered, revealing the characteristic "mist" and "twist hackle".[1] Beauchamp[2] found that all three regions are self-similar. The primary fractographic difference between these regions is the progressively larger length scale, from mirror and mist to twist hackle.[3,4] corresponding to increasing crack tip velocities. Constant surface roughness contours, such as boundaries between these optically distinct regions, therefore represent a convenient method for identifying SIF loci.

Figure 1(a) provides a schematic view of a sample fractured in bending, showing common SIF loci. The mirror radius, R_m, and the twist hackle radius, R_o, are distances along the free surface for these two particular SIF loci. The angle between the free surface on the tension side of the sample and a SIF locus, such as the mirror-mist boundary, is defined as θ_m.

The fracture strength, σ_f, has often been correlated to characteristic length scales by a material parameter, A_m, by Orr's equation:[5]

$$\sigma_f = A_m \Big/ \sqrt{R_m} + \sigma_0 \tag{1}$$

Orr originally did not include the term σ_0 shown in Equation 1, although this is a common modification. In the absence of residual stresses, the term σ_0 is equal to zero for tensile samples and is generally negligible for thick samples failed in bending. Although Orr's equation is accurate for most bulk applications, it becomes increasingly inaccurate in bending as the sample's thickness decreases as also noted by both Shand[6] and Kirtchner *et al.*[7] Dugnani and Zednik[8] showed that a more general expression that also applies to thin geometries is given by:

$$\begin{aligned}\sigma_f &= A_{md} \Big/ \sqrt{R_m} \\ &= K_{Im}\left[2.02 - 1.20\exp\left(-0.459\frac{R_m}{H}\right)\right] \Big/ \sqrt{R_m} \text{ for } R_m < 4H\end{aligned} \tag{2}$$

The term K_{Im} is the Mode I SIF for the locus considered, and A_{md} refers to a dynamic parameter that depends on the specimen's thickness, H. This model applies to the SIF loci in any brittle, isotropic material, as the classical fracture mechanics expressions used in the derivation are mechanism independent; the numerical values in this expression are geometrical parameters derived from dynamic computational fracture mechanics for a beam in pure bending.

II. Calculation of SIF Locus Angle

Considering a beam specimen with a rectangular cross section loaded in pure bending, the stress profile at failure can be written as

T. Rouxel—contributing editor

Manuscript No. 34922. Received April 28, 2014; approved August 26, 2014.
[†]Author to whom correspondence should be addressed. e-mail: roberto.dugnani@sjtu.edu.cn

$$\sigma(y) = \sigma_f(1 - 2y/H) \tag{3}$$

The radius from the crack origin along the free surface to a given SIF locus, such as the radius of the mirror region, R_m, can be expressed in terms of a dynamic parameter, A_{md}, and the fracture strength, σ_f, through Equation 2:

$$R_m = A_{md}^2 \Big/ \sigma_f^2 \tag{4}$$

At the limit $y = \delta y$, the radius to a given SIF locus, $r_m(\delta y)$, also runs parallel to the surface, as illustrated schematically in Fig. 1(b). Combining Equations 3 and 4,

$$\begin{aligned} r_m(y)|_{y=\delta y} &\approx \frac{\left(A_{md} + \delta A_{md}\right)^2}{\bar{\sigma}^2} \\ &= \frac{A_{md}^2\left(1 + \delta A_{md}^2/A_{md}^2 + 2\delta A_{md}/A_{md}\right)}{\sigma_f^2(2\cdot\delta y/2H - 1)^2} \\ &= \frac{R_m\left(1 + \delta A_{md}^2/A_{md}^2 + 2\delta A_{md}/A_{md}\right)}{(\delta y/H - 1)^2} \end{aligned} \tag{5}$$

The term δA_{md} accounts for the small change in the crack shape at a depth δy away from the free surface. The difference in the crack length at the SIF locus along the free surface at a depth δy is denoted by δr:

$$\begin{aligned} \delta r &= r_m(\delta y) - R_m \\ &= R_m\left[\frac{1 + \delta A_{md}^2/A_{md}^2 + 2\delta A_{md}/A_{md}}{(\delta y/H - 1)^2} - 1\right] \end{aligned} \tag{6}$$

Taking the limit of δr as $\delta y \to 0$,

$$\lim_{\delta y \to 0} \delta r = R_m \cdot \left(\delta A_{md}^2/A_{md}^2 + 2\delta A_{md}/A_{md} + 2\delta y/H\right) \tag{7}$$

The tangent of θ_m is given by the ratio $\delta y/\delta r$ for an infinitesimally small distance from the surface δy. The ratio $\delta A_{md}/A_{md} \ll 1$, and hence the quadratic term in Equation 7 becomes negligible:

$$\begin{aligned} \tan\theta_m|_{y=\delta y} &= \frac{\delta y}{\delta r} = \frac{\delta y}{2\frac{R_m}{H}\delta y\left[\frac{H}{A_{md}}\frac{\partial A_{md}}{\partial y} + 1\right]} \\ &= \frac{H}{2R_m}\left(\frac{1}{\frac{H}{A_{md}}\frac{\partial A_{md}}{\partial y} + 1}\right) = \frac{H}{2R_m}\left(1 - \frac{\frac{H}{A_{md}}\frac{\partial A_{md}}{\partial y}}{\frac{H}{A_{md}}\frac{\partial A_{md}}{\partial y} + 1}\right) \\ &= \frac{H}{2R_m} - \frac{\hat{\Psi}^2}{2} = \frac{H\cdot\sigma_f^2}{2A_{md}^2} - \frac{\hat{\Psi}^2}{2} = \frac{\Psi^2}{2} - \frac{\hat{\Psi}^2}{2} \end{aligned}$$

$$\begin{aligned} \because \hat{\Psi}^2/2 &= H/(2R_m)\frac{H/A_{md}\partial A_{md}/\partial y}{H/A_{md}\partial A_{md}/\partial y + 1} \\ &= H/(2R_m)\frac{H/A_{md}\partial A_{md}/(R_m\partial\theta)}{H/A_{md}\partial A_{md}/(R_m\partial\theta) + 1}; \end{aligned}$$

$$\Psi \equiv \sqrt{H}\cdot\sigma_f \Big/ A_{md} = \sqrt{H/R_m} \tag{8}$$

Equation 8 can be written explicitly in terms of the angle θ_m,

$$\theta_m = \arctan\left[\left(\Psi^2 - \hat{\Psi}^2\right)\Big/2\right] \quad \text{with} \quad \hat{\Psi} \equiv \sqrt{H}\cdot\hat{\sigma}_f \Big/ A_{md} \tag{9}$$

The term Ψ is the nondimensionalized fracture strength, such that $\Psi = \hat{\Psi}$ when θ_m is zero. The term $\hat{\Psi}$ therefore corresponds to the critical stress $\hat{\sigma}_f$ necessary for forming the SIF locus.

For long cracks, the crack front has been reported to maintain a nearly constant shape,[9] hence both $\partial A_{md}/\partial\theta$ and A_{md} are expected to be relatively constant. Also, $\partial A_{md}/\partial\theta > 0$, because the SIF is larger at the free surface.[10] It follows that $\hat{\Psi}$ is positive and relatively constant, regardless of the thickness, H, or the material properties of the sample. It should be noted that the expressions derived above only apply to amorphous materials as for crystalline solids there is a dependency between the mirror constant and the relative propagation direction, θ, and hence the assumptions made in the derivation of Equation 9 do not apply.

III. Experimental Validation

Four-point bending (4PTB) tests were carried out on isotropic brittle samples to confirm the validity of our method and illustrate a technologically useful implementation of such an analysis. Samples were tested to measure their flexural strength; the strength was correlated with the shape of SIF loci determined by inspecting the fracture surfaces using optical microscopy. In this case, the mirror-mist boundary was taken as the SIF locus of interest, so that θ_m and R_m represent the mirror-mist angle and the mirror radius, respectively. The 4PTB tests were conducted on aluminosilicate glass (ASG) (140 samples each 1.0 mm thick, 28 samples each 0.7 mm thick) and borosilicate glass (BSG) (35 samples each 0.7 mm thick and 12 samples each 0.3 mm thick). These materials were selected as model material systems due to their technological importance, although any isotropic brittle material could have been chosen. For all samples, no edge treatment or heat treatment was performed prior to the 4PBT. A loading rate of 1.1 ± 0.1 MPa/s was used. The tests were performed on an Instron universal pull tester (load cell resolution of 0.01 N).

In this case, the value of θ_m in Equation 9 was defined as the angle between the free surface and loci on the fracture surface having a constant SIF. The mirror-mist boundary used in the experimental validation is merely an optically convenient fractographic artifact that corresponds to one particular value of the SIF. Equation 9 also applies to other values of the SIF, such as, for instance, the one corresponding to the mist-hackle boundary region. Since Equation 9 is not bound by specific values of the SIF, it is valid regardless of the material and any corresponding locus may be selected.

Figure 2 illustrates the experimental results obtained. The square root of the thickness of the sample normalized by the mirror radius, $\sqrt{(H/R_m)}$, is plotted on the ordinate axis while the abscissa shows the angle of the mist region, θ_m. In addition to the tests performed by the authors, additional measurements were taken on fracture images reported in the literature.[11,12]

A constant value for the nondimensional parameter, $\hat{\Psi} = 0.5$, was used for the analytical trend in the plot. Such value was estimated based on Equation 8 using the measured mirror radius and sample thickness for those fractured samples where the angle of the mist approached zero. It was found that a slightly improved fit between the test data and the analytical trend can be achieved by multiplying the angle of the mirror boundary region, θ_m, by an empirical fitting constant of 1.1:

$$\tan(1.1\cdot\theta_m) \cong H/(2R_m) - 0.125 \quad \text{for} \quad \sqrt{H/R_m} < 2.5 \tag{10}$$

Recalling that $H/R_m = H\sigma_f^2 \Big/ A_{md}^2$, we obtain an expression for the fracture strength:

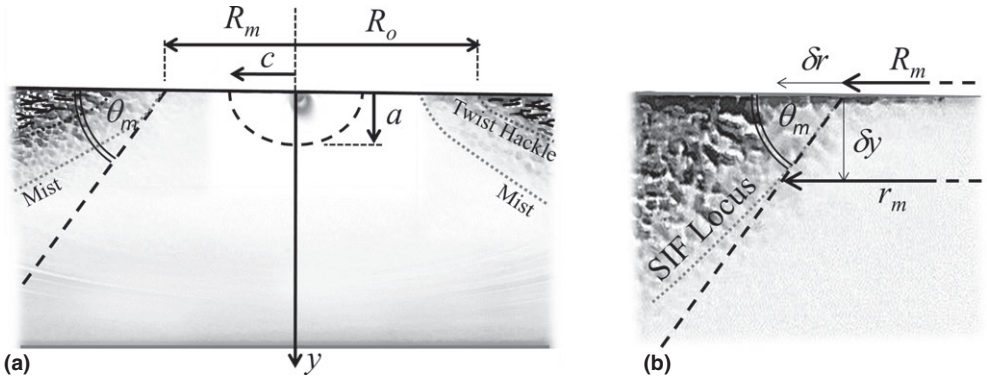

Fig. 1. (a) Geometric parameters for a typical brittle fracture surface failed in bending, and (b) Schematic of the dimensions related to the calculation of SIF locus angle θ_m.

$$\sigma_f \cong A_{md}\sqrt{2[\tan(1.1\cdot\theta_m)+0.125]/H} \quad \text{for} \quad \sqrt{H/R_m}<2.5 \tag{11}$$

The analytical solution accurately tracks the experimental data for $\sqrt{H/R_m}<2.5$. Since no mist is expected to occur for R_m larger than $4H$, it follows that Equation 11 is applicable in the range $0.16H < R_m < 4H$. The improved fit provided by employing an empirical fitting constant close to unity is likely attributed to the fact that the mirror-mist angle at the surface is affected by the presence of residual compressive surface stresses typically found in glass. These compressive residual stresses would reduce the effective surface stress, hence making the mirror-mist angle shallower than the predicted value computed analytically.

IV. Discussion of Experimental Illustration

One implication of the mirror-mist angle analysis presented in the previous section is that a minimum mechanical stress is necessary for the formation of the mist region. Intuitively, as the fracture stress decreases, the angle of the mirror-mist boundary also decreases. Ultimately, at a critical value of the stress, $\hat{\sigma}_f$, the angle of the mirror-mist region becomes too shallow to be detected. The existence of a minimum stress necessary for the formation of the mist region is predicted analytically (Equation 9).

Figure 3 is a summary plot showing the minimum stress level necessary for the mirror-mist boundary region to form in various glass samples. Thresholds were obtained at values of the nondimensional stress equal to $\hat{\Psi} = 0.5$.

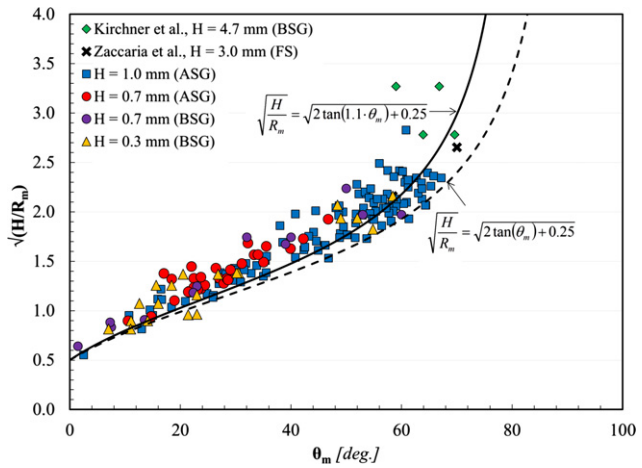

Fig. 2. Square root of the thickness over the mirror radius, $\sqrt{H/R_m}$, versus the mirror-mist angle, θ_m.

An explicit expression for the minimum critical stress for mirror formation is obtained by combining the results from Equations 2 and 9:

$$\hat{\sigma}_f = \hat{\Psi}\cdot K_{Im}\Big/\sqrt{H}\Big[2.02 - 1.20\exp\Big(-0.459\Big/\hat{\Psi}^2\Big)\Big] \tag{12}$$

Equation 12 indicates that $\hat{\sigma}_f$ is only a function of the sample thickness, H, and the SIF of the material at the onset of the mist region, K_{Im}, since $\hat{\Psi} \approx 0.5$ is a geometric term largely independent of the material properties. An important practical consequence of this analysis is that Equation 12 enables materials scientists to set an upper limit for the stress in a material when no mist formation occurs. This result might seem trivial for thick geometries, where very often the absence of mist in a fractured sample implies low stress at failure. Nonetheless, this is extremely important for thin geometries of brittle materials that may experience large mechanical loads.

V. Characterizing Inhomogeneous Stress Fields

One implication of this generalized method is that, when coupled with traditional stress characterization techniques, it allows determination of inhomogeneous stress fields present in the specimen. Such inhomogeneous stress fields can be the result of residual stresses or surface treatments. For example, measurements of the mirror-mist angle can be used to discriminate whether the sample failed due to pure bending

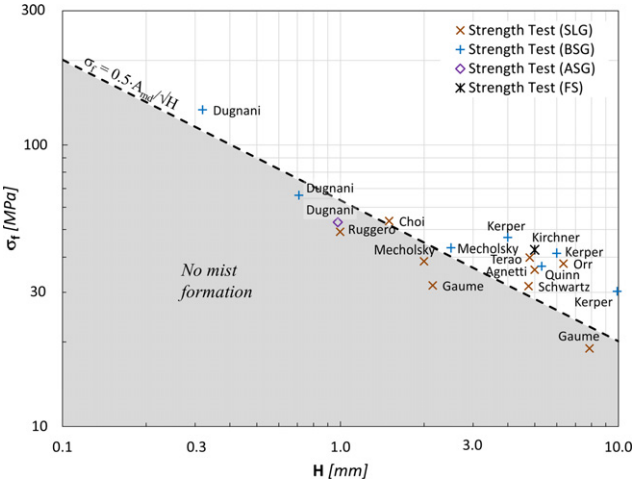

Fig. 3. Minimum stress level, $\hat{\sigma}_f$, required for the mirror-mist boundary region to form versus sample thickness ($\hat{\Psi} = 0.5$). Minimum reported glass strength, σ_f, for various sample thicknesses is also shown for reference.

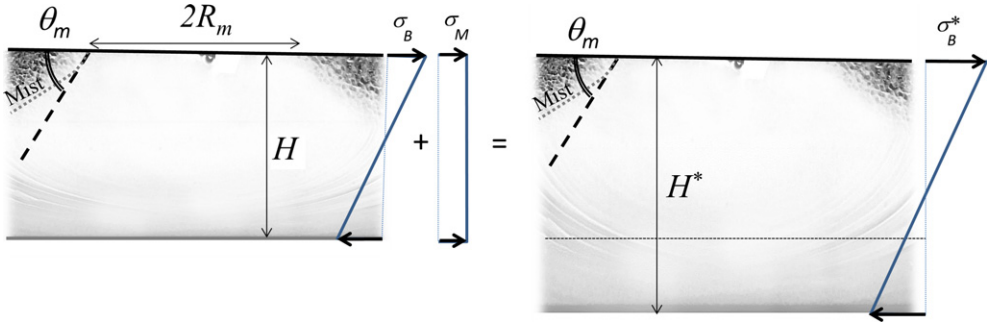

Fig. 4. Schematic view of the equivalent bending stress and equivalent glass thickness H^*.

loads alone or whether inhomogeneous stresses (e.g., membrane stresses due to surface treatment) were also present.

Equation 11 relates the stress at failure to the angle formed by the mirror-mist boundary with the free surface; this expression only applies to samples loaded in pure bending. If both bending stresses and membrane or surface stresses are present in the sample, the stress gradient remains unchanged but the location of the neutral axes shifts from the centroid of the cross section to a new location at distances $H^*/2$ and $(H-H^*/2)$ from the surfaces of the sample. For the case when both tension and bending loads are applied to the sample, the location of the neutral axis can be obtained from the equilibrium equations. Since the analysis outlined in the previous sections considers pure bending stresses only, it is convenient to define an equivalent bending stress field and an equivalent sample thickness H^*. The equivalent bending stress field is obtained by realizing that the stress field for a sample of thickness H^*, loaded in pure bending, would produce the same effective stress profile along the fracture origin surface as the original sample of thickness H loaded both in tension and bending.

Figure 4 shows a schematic view of how the value of the equivalent sample thickness H^* can be obtained. On the actual sample shown on the left-hand side in Fig. 4, the stress distribution is given by the superposition of the uniform membrane stress, σ_M, and bending stress, σ_B, at the surface. Hence the inhomogeneous stress profile is given by:

$$\sigma(y) = (1 - 2y/H)\sigma_B + \sigma_M \tag{13}$$

The stress distribution for the equivalent sample in pure bending is given by:

$$\sigma^*(y) = (1 - 2y/H)\sigma_B^* \tag{14}$$

Since the stress at the surfaces (i.e., $y = 0$ and $y = H$) needs to be identical for both stress profiles, it follows that the membrane stress, σ_M can be calculated as:

$$\sigma_M = (1 - H/H^*)(\sigma_B + \sigma_M) = (1 - H/H^*)\sigma_f \tag{15}$$

If both the mirror radius, R_m, and the angle of the mirror-mist boundary region, θ_m, are known, then Equation 10 can be used to calculate H^* for the equivalent bending stress. Since $\sigma_f = \sigma_B + \sigma_M$, it is possible to estimate the stress field near the surface of the fractured sample.

VI. Conclusions

This manuscript introduces a generalized method for quantitatively characterizing the mechanical stresses present in isotropic brittle materials based on SIF loci during crack tip propagation. This approach was derived exclusively from classical fracture mechanics arguments and is therefore mechanism and material independent: it applies to a wide range of systems, including glasses, fine grained ceramics or metals, and high stiffness polymers. An experimental implementation of this analytical technique involves determining the fracture strength of a beam in bending during a brittle overload event fracture surface artifacts corresponding to SIF loci. Inhomogeneous stress fields present in the material can also be analyzed by combining this novel method with traditional stress characterization techniques.

References

[1]W. H. Duckworth, D. K. Shetty, A. R. Rosenfeld, and W. R. Siskos, "Influence of Stress Gradients on the Relationship Between Fracture Stress and Mirror Size for Float Glass," *Glass Technol.*, **24** [5] 263–73 (1983).
[2]E. K. Beauchamps, Sandia Laboratories Research Report, SC-RR-70766 (1971).
[3]D. Hull, "Influence of Stress Intensity and Crack Speed on Fracture Surface Topography: Mirror to Mist Transition," *J. of Mat. Science*, **3** 1829–41 (1996).
[4]E. Sharon and J. Fineberg, "Confirming the Continuum Theory of Dynamic Brittle Fracture for Fast Cracks," *Nature*, **397** 333–5 (1999).
[5]L. Orr, "Practical Analysis of Fractures in Glass Windows," *Mater. Res. Stand*, **12** [1] 21–3 (1972).
[6]E. B. Shand, "Breaking Stress of Glass Determined From Dimensions of Fracture Mirrors," *J. Am. Ceram. Soc.*, **42** [10] 474–7 (1959).
[7]H. P. Kitchner and J. C. Conway, "Comparison of the Stress-Intensity and Johnson-and-Holloway Criteria for Crack Branching in Rectangular Bars," *J. Am. Ceram. Soc.*, **70** [8] 565–9 (1987).
[8]R. Dugnani and R. Zednik, "Flexural Strength by Fractography in Modern Brittle Materials," *J. Am. Ceram. Soc.*, **96** [12] 3908–14 (2013).
[9]D. Sherman and I. Be'ery, "Shape and Energies of a Dynamically Propagating Crack Under Bending," *J. Mater. Res.*, **18** [10] 2379–86 (2003).
[10]J. C. Newman and I. S. Raju, "An Empirical Stress-Intensity Factor Equation for the Surface Crack," *Eng. Fract. Mech.*, **15** [1–2] 185–92 (1981).
[11]H. P. Kirchner and J. W. Kirchner, "Fracture Mechanics of Fracture Mirrors," *J. Am. Ceramic Society*, **62** [3–4] 198–202 (1979).
[12]M. Zaccaria and M. Overend, "Validation of a Simple Relationship Between the Fracture Pattern and the Fracture Stress of Glass," Engineered Transparency. International Conference at Glasstec, Düsseldorf, Germany, 25-26 October 2012. □